



Numerical study of fuel-clad mechanical interaction during long-term burnup of WWER1000

Morteza Imani, M. Aghaie *, A. Zolfaghari, A. Minuchehr

Engineering Department, Shahid Beheshti University, G.C., P.O. Box: 1983963113, Tehran, Iran



ARTICLE INFO

Article history:

Received 24 May 2014

Received in revised form 19 January 2015

Accepted 20 January 2015

Available online 26 February 2015

Keywords:

Fuel rod
Finite element
Virtual work
Swelling
Creep
WWER1000

ABSTRACT

Thermo-mechanical behavior of fuel rod is of great importance for safety assessment of nuclear reactors. This paper deals essentially with the mechanical description of pressurized water reactor (PWR) fuel rods under long-term burnups. The main goal of the work is generation of a numerical code for study of pellet-cladding interaction (PCI) as long-term phenomena in Bushehr nuclear power plant (BNPP). In this way, a basic modeling hypothesis with particular attention being paid to the numerical treatment of stress relaxation and interaction of fuel swelling and clad creep down have been implemented. In this model, the mechanical equilibrium equations are integrated on principle of virtual work with generalized plane strain assumption and the numerical algorithm is based on finite element method. Afterward, the generated code, IR-FRA (Iranian Fuel Rod Analysis), is developed for long-term behavior study of fuel rods. For validating the IR-FRA code, the pellet-cladding interaction results in some test cases are compared with the FROBA, BISON codes and experimental data. These comparisons demonstrated the accuracy and capability of the presented code for prediction of fuel rods thermo-mechanical behavior. Eventually, the fuel and cladding mechanical interaction during long-term burnup of WWER1000 for the BNPP is simulated and results show good agreement with experimental and published data.

© 2015 Elsevier Ltd. All rights reserved.

1. Introduction

The core power range of PWR reactor is limited by departure from nucleate boiling, fuel melting and pellet-clad interaction (PCI), etc. hence description of the mechanical and thermal behaviors of fuel rods is essential to design and operation specification of the reactor core. Due to constantly increasing demands on reactor fuel efficiency, the development of new fuel rods with new materials and the reliability of these new fuel rods are also interests of fuel vendors and fuel designer to analyze the performance of this new fuel designs. The prediction of light water reactor (LWR) fuel rods behavior under long-term burnup conditions is a major objective of the reactor safety analysis. In this way, development of a computer code that simulates thermal and mechanical behaviors such as fuel swelling, fuel densification, cladding creep down, thermal expansion, temperature profiles, etc. helps to accurate prediction. Development of such codes is an interest of the nuclear fuel and material researchers. Many computer codes have been developed recently. The steady-state single-rod codes, like FRAPCON, TRANSURANUS, COMETHE, and FEMAXI-V calculate thermal

quantities such as radial temperature profile, fission gas release to the gap, mechanical quantities such as creep deformation, and irradiation growth. Results are used for many purposes like axial clearance between rods and end fittings, internal gas pressure to compare with system pressure, cladding oxide thickness to compare with established limits or to initiate transient calculations, stored energy for LOCA (loss of coolant accident) analysis, fission gas repartition between grains, grain boundaries, and porosities for RIA (reactivity initiated accident) fuel failure mechanisms studies. These codes consist of models and correlations to describe gap conductance, material properties such as thermal conductivity and specific heat, radial power profiles, stress-strain equations, mechanical properties, creep properties, fuel swelling, fuel-densification, waterside corrosion, and hydrogen absorption (Hikmet and Pedro, 2005). The existing codes also have some limitations or disadvantages. For instance, many thermal correlations in FEMAXI-V are not valid for high-burnup condition and some of the correlations are even independent from burnup. Compared with FEMAXI-V, the correlations in FRAPCON-3 code are functions of burnup and valid for various burnup conditions. But the rigid-fuel model used in FRAPCON-3 code assumes that the thermal expansion and the fuel restructuring are the only sources of fuel deformation and that the cladding provides no resistance to fuel expansion (Yu et al., 2012). In this work, a computer code is devel-

* Corresponding author. Fax: +98 02122431595.

E-mail address: M_Aghaie@sbu.ac.ir (M. Aghaie).

Nomenclature

A	a parameter describing enhancement of the cladding oxidation rate in a reactor environment	h	gap conductance ($\text{W}/(\text{m}^2 \text{ K})$)
Bu	fuel burnup (MWd kg^{-1})	h_f	coolant conductance ($\text{W}/(\text{m}^2 \text{ K})$)
Bu_1	input burnup to end of last time step ($\text{MW}\cdot\text{s}/\text{kg-U}$)	h_{gas}	conduction through the gas ($\text{W}/(\text{m}^2 \text{ K})$)
C	constant in contacted gap conductance formula; constant in creep model, 15,000	h_{rad}	radiation from fuel to cladding ($\text{W}/(\text{m}^2 \text{ K})$)
D	pellet density in early life (kg m^{-3}), diffusion coefficient ($\text{m}^{-2} \text{ s}^{-1}$); matrix relating the total stress vector and the elastic strain vector	h_{solid}	conduction through points of contact ($\text{W}/(\text{m}^2 \text{ K})$)
D_e	coolant channel heated diameter (m)	k_c	conductivity of cladding ($\text{W}/(\text{m K})$)
G	coolant mass flux (kg/s m^2)	k_f	conductivity of fuel ($\text{W}/(\text{m K})$)
H	Meyer hardness (pa)	k_{gas}	gas thermal conductivity ($\text{W}/(\text{m K})$)
K_m	mean conductivity ($\text{W}/(\text{m k})$)	p	coolant pressure (pa)
P_c	interfacial pressure (pa)	$q''(z)$	rod surface heat flux at elevation z in the rod axial direction (W/m^2)
Pr	Prandtl number	r_i	cladding inside radius (m)
Re	Reynolds number	r_o	cladding outside radius (m)
S_{solid}	Solid fission product swelling	t	time at temperature (days); time in creep model (h)
S_{gas}	Swelling due to gaseous fission products		
T	temperature of the oxide-metal interface (K)		
X_{tran}	thickness of the oxide layer at transition point (m)		
X_{post}	thickness of the oxide layer when the oxide film is in the post transition state (m)		
X_0	the initial oxide thickness (m)		
X_{pre}	thickness of the oxide layer when a pre transition oxide film exists (m)		
a	grain size (m); constant in creep model, 300		
b	body force; constant in creep model, 2.95		
d	open fuel-cladding gap size (m); constant in creep model, $2.8 * 10^{-22}$		
d_{eff}	effective gap width (m)		
f_c	the release fraction of fission gas		
f_s	surface force acting on the body		
g_f	temperature jump distance at fuel surface (m)		
g_c	cladding inside temperature jump distance (m)		
<i>Greek characters</i>			
	δ	mean thickness of the gas space	
	ε	strain component	
	ε_f	fuel emissivity	
	$\dot{\varepsilon}_0$	the creep hoop strain rate	
	σ	Stefan-Boltzmann constant, $5.6697 * 10^{-8}$ ($\text{W}/(\text{m}^2 \text{ K}^4)$); stress component	
	σ^{cr}	vector containing 'crack stress' components	
	ρ	density (kg/m^3)	
	ϕ	the fast neutron flux ($\text{n}/(\text{m}^2 \text{ s})$)	
<i>Subscripts and superscripts</i>			
	D	strain due to densification	
	c	clad	
	el	elastic strain	
	f	fuel	
	$n.el$	non-elastic	
	r	radial direction	

oped (IR-FRA) to predict the steady state long-term burnup behavior of fuel rod in PWRs. This code consists of three parts. The thermal analysis, which calculates temperature distribution of fuel pellet and clad in radial direction and coolant temperature in axial direction. The mechanical analysis, which calculates stress, strain, and displacement in fuel pellet and clad in radial direction, swelling and densification of fuel pellet, pellet-cladding interaction, and thermal expansion. The third part is the material properties subroutine, which include water properties, conductivity and mechanical properties of clad and fuel pellet. In mechanical part of code, the principle of virtual work is used for derivation of equilibrium equations and the finite element method, is applied for numerical solution. Also, new correlation for cladding creep down is applied. For validating the reliability and accuracy of the IR-FRA code, the pellet-cladding interactions have been simulated and results are compared with FROBA (Hongxing et al., 2012) and BISON (Williamson, 2010) codes. These comparisons showed the accuracy and applicability of the presented code for prediction of fuel rods thermo-mechanical behavior. Finally, the fuel and cladding interactions during long-term burnup of WWER1000 for the BNPP were simulated and results showed good agreement with experimental data.

2. Brief description of fuel rod model

The fuel rod geometry is represented by cylindrical fuel pellets, which are located symmetrically within a cylindrical clad tube. The clad tube is surrounded by coolant, as shown in Fig. 1. In addition, a

gas plenum volume is assumed at the top of the fuel rod. Fuel rod heat transfer and deformations are calculated for each axial segment individually, neglecting heat transfer and mechanical forces between adjacent segments. This simplification, in combination with the assumed axial symmetry, makes the governing equations one-dimensional, for heat transfer and deformation. The IR-FRA code calculation flow diagram is shown in Fig. 2.

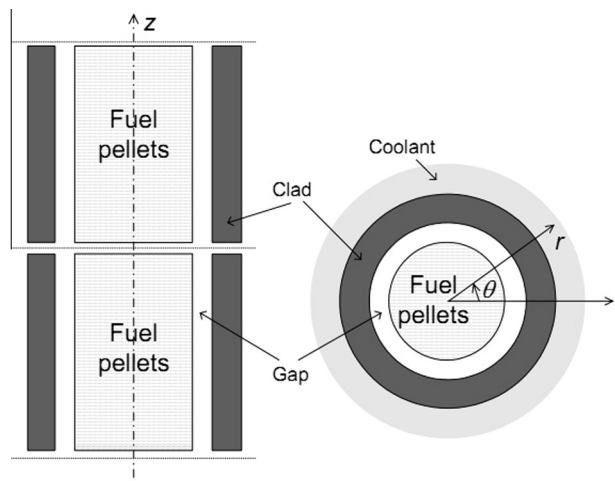


Fig. 1. Geometrical representation of the fuel rod.

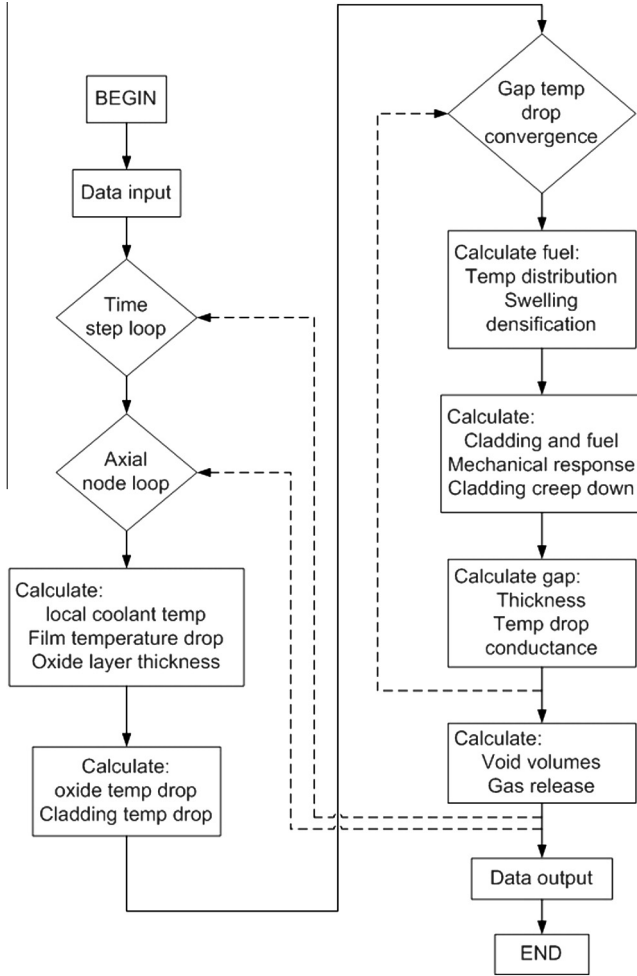


Fig. 2. Calculation flow diagram of the IR-FRA code.

2.1. Thermal response

The thermal analysis consist determination of the radial temperature distribution in each axial segment of the fuel rod, as schematically showed in Fig. 3.

Bulk coolant temperature is calculated in each axial segment then heat transfer between coolant and outer surface of oxide layer

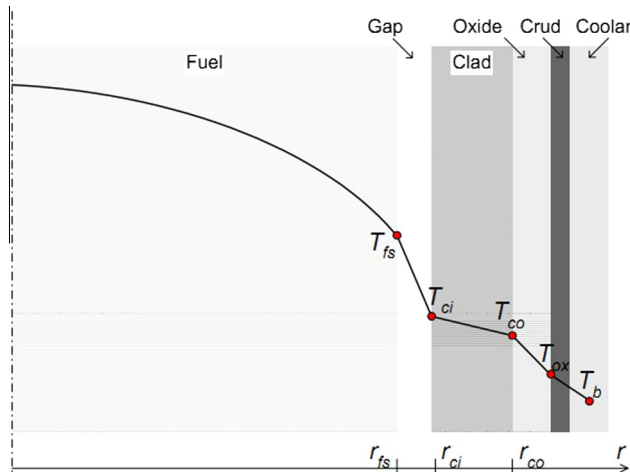


Fig. 3. Schematic radial temperature profile.

is applied by Dittus–Boelter correlation for single-phase flow with Eq. (1). In two phase flow case, bulk coolant temperature is obtain from Jens–Lottes correlation with Eq. (2) (Berna et al., 1997):

$$h_f = (0.023k/D_e)Re^{0.8}Pr^{0.4} \quad (1)$$

$$\Delta T_{JL}(z) = 60 \left[q''(z)/10^6 \right]^{0.25} / e^{(p/6.2 \times 10^6)} \quad (2)$$

2.1.1. Cladding and oxide layer thermal models

For calculating temperature drop across the zirconium oxide layer, the oxide layer thickness is required. For calculating oxide layer thickness, it should be considered that cladding oxidation properties depend on the oxide thickness and to some extent on the temperature of the oxide. For thin oxides, the rate of oxidation is controlled by the entire oxide layer. When the oxide layer becomes thicker, a change of the outer portion occurs; and further oxidation is controlled by the intact inner layer. The transition between stages is described in terms of thickness of the oxide layer at transition with Eq. (3) (Allison et al., 1993). For pre-transition and post-transition the thickness is calculated with Eqs. (4) and (5), respectively:

$$X_{tran} = 7.749 * 10^{-6} \exp \left(-\frac{790}{T} \right) \quad (3)$$

$$X_{pre} = \left[4.976 * 10^{-9}(At) \exp \left(-\frac{15,660}{T} \right) + X_0^3 \right]^{1/3} \quad (4)$$

$$X_{post} = 82.88A(t - t_{tran}) \exp \left(-\frac{14,080}{T} \right) + X_{tran} \quad (5)$$

The cladding temperature drop for each axial segment is calculated according to Eq. (6) (Berna et al., 1997):

$$\Delta T_c = \frac{q''(z)r_o \ln(r_0/r_i)}{k_c} \quad (6)$$

2.1.2. Pellet to clad gap

The model for heat transfer across the pellet to clad gap consist of three different heat transport mechanisms; conduction through the gap gas, pellet to clad radiation, and pellet to clad contact conduction:

$$h = h_{rad} + h_{gas} + h_{solid} \quad (7)$$

The pellet to clad radiation conductance is calculated by Kreith with Eq. (8) (Berna et al., 1997). The conductance through the gas gap is calculated by Ross–Stoute model with Eq. (9) (Ross and Stoute, 1962) and conductance due to pellet-clad contact is described using the empirical model suggested by Olander with Eq. (10) (Todreas and Kazimi, 1999):

$$h_{rad} = \left(\frac{\sigma}{1/\varepsilon_f + 1/\varepsilon_c - 1} \right) \frac{T_f^4 - T_c^4}{T_f - T_c} \quad (8)$$

$$h_{gas} = \frac{k_{gas}}{d_{eff} + d + (g_f + g_c)} \quad (9)$$

$$h_{solid} = C \frac{2k_f k_c}{k_f + k_c} \frac{P_c}{\delta^{1/2} H} \quad (10)$$

2.1.3. Pellet thermal models

For numerical investigations, the differential equation for heat transfer is solved over the cylindrical geometry, accounting the radial heat fluxes in the pellet:

$$\rho c \frac{\partial T}{\partial t} = \frac{1}{r} \frac{\partial}{\partial r} \left(\lambda r \frac{\partial T}{\partial r} \right) + q''' \quad (11)$$

The conductivity of un-irradiated fuel is corrected for operation conditions in reactor which described in detail in [Lucuta et al. \(1996\)](#). For instance, the conductivity of irradiated fuel for several burnup is showed in [Fig. 4](#).

2.2. Mechanical analysis

Computing stress and strain fields in fuel and clad is essential for modeling the behavior of fuel rods, especially under pellet-cladding interaction conditions ([Garcia et al., 2002](#)). Therefore, the accurate calculation of fuel and clad deformation is necessary. In this way, a mechanical model is applied, in which mechanical equilibrium equations were derived from the principle of virtual work and solved with finite element method. Applying some modification to described method, this model has been utilized in this code.

2.2.1. Displacement calculation

The principle of virtual work states that the stress, body force, and traction are in equilibrium if and only if the internal virtual work equals the external virtual work for every virtual displacement field. Mathematically, this is expressed by the following equation ([Garcia et al., 2002](#)):

$$\int_V \sigma : \delta e dV = \int_s f_s \delta u_i dS + \int_V b \delta u_i dV \quad (12)$$

The second term in right side of Eq. (12) is considered equal to zero in this case (body forces). For derivation of Eq. (12) the relation between stresses and strains is given by:

$$\sigma = D e^{el} \quad (13)$$

where D is the matrix expression of the elasticity tensor:

$$D = \frac{E}{(1+\nu)(1-2\nu)} \begin{pmatrix} 1-\nu & \nu \\ \nu & 1-\nu \end{pmatrix} \quad (14)$$

The total strain assumed to be obtained by summing elastic and non-elastic strain:

$$e = e^{el} + e^{n.el} \quad (15)$$

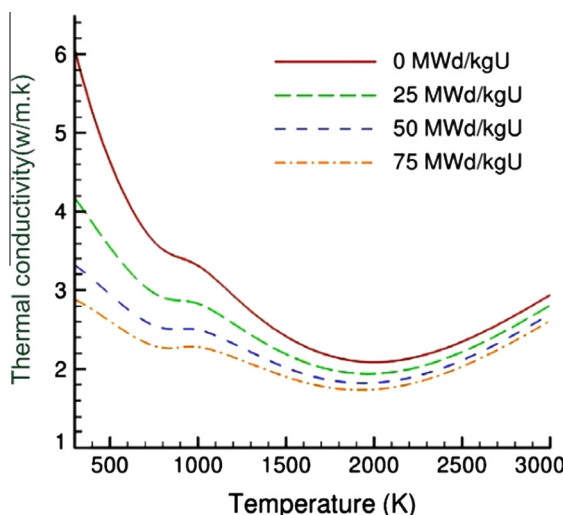


Fig. 4. Burnup dependent thermal conductivity of UO_2 via temperature ([Williamson, 2011](#)).

The strains in the r and θ directions are related to the radial displacement field u , by the following relations:

$$\begin{pmatrix} \varepsilon_r \\ \varepsilon_\theta \end{pmatrix} = \begin{pmatrix} \frac{\partial u}{\partial r} \\ \frac{u}{r} \end{pmatrix} = \begin{pmatrix} \frac{u_j - u_i}{r_j - r_i} \\ \left(\frac{1 - \frac{r_i}{r}}{r_i - r_j}\right) u_i + \left(\frac{1 - \frac{r_i}{r}}{r_j - r_i}\right) u_{i+1} \end{pmatrix} \quad (16)$$

By replacing Eq. (16) into Eq. (15) and substituting it into Eq. (13), the Eq. (12) for a local element obtained. This equation is numerical form of Eq. (12) for local element:

$$\begin{aligned} & \int_{r_i}^{r_j} \begin{pmatrix} -1 & \left(\frac{r_i}{r} - 1\right) \\ 1 & \left(1 - \frac{r_i}{r}\right) \end{pmatrix} D_{2x2} \begin{pmatrix} -1 & 1 \\ \left(\frac{r_i}{r} - 1\right) & \left(1 - \frac{r_i}{r}\right) \end{pmatrix} \begin{pmatrix} u_i \\ u_j \end{pmatrix} 2\pi r dr \\ &= L \int_{r_i}^{r_j} \begin{pmatrix} \varepsilon_r^{n.elas} \\ \varepsilon_\theta^{n.elas} \end{pmatrix}^t D_{2x2} \begin{pmatrix} -1 & 1 \\ \left(\frac{r_i}{r} - 1\right) & \left(1 - \frac{r_i}{r}\right) \end{pmatrix} 2\pi r dr \end{aligned} \quad (17)$$

It could be seen from Eq. (17) that the displacement in each desired node could be evaluated numerically. A set of linear equation could be obtained from Eq. (17) for radial elements. The displacement field $[u]$ should be obtained by solving the system of assembled linear equations in general form. The evaluated displacement matrix could be used to calculate the strain and stress values over the entire continuum.

2.2.2. Swelling

The solid and gaseous fission products cause fuel swelling. So the empirical correlations from MATPRO are used for considering this effect ([Allison et al., 1993](#)).

For the solid fission product:

$$S_{solid} = 7.435 * 10^{-13} \cdot D \cdot (Bu - Bu_1) \quad (18)$$

For the gaseous fission product:

$$S_{gas} = 2.617 * 10^{-39} \cdot D \cdot (Bu - Bu_1) \cdot (2800 - T)^{11.73} \cdot e^{(-0.0162 \cdot (2800 - T))} \cdot e^{(-2.4 * 10^{-10} \cdot Bu \cdot D)} \quad (19)$$

2.2.3. Densification

Fuel densification is a phenomenon that rapidly removes as-fabricated internal porosity when fuel pellets are irradiated in a reactor. Fuel densification is computed using the ESCORE model given by ([Kramman and Freeburn, 1987](#)):

$$\varepsilon_D = \Delta \rho_0 \left(e^{\frac{Bu - \ln(0.01)}{C_D B_D}} - 1 \right) \quad (20)$$

2.2.4. Cladding creep down

Cladding diametrical creep during normal operation and operational transients influences the pellet-cladding gap thickness and pellet-cladding mechanical interaction (PCMI) contact force. Since these have a direct impact on fuel pellet temperatures, cladding creep is an important mechanism to include in a fuel performance modeling code ([Rashid et al., 2004](#)). Cladding creep down is computed using the CIEMAT model given by ([Herranz and Feria, 2010](#)):

$$\dot{\varepsilon}_\theta = f_1(\sigma_\theta) f_2(T) f_3(\phi t) t^{-0.5} \quad (21)$$

where

$$f_1(\sigma_\theta) = 1/2a\sigma_\theta^b$$

$$f_2(T) = \exp\left(\frac{-c_3}{T_{clad} + 273}\right)$$

$$f_3(\phi t) = \exp(-c_4 \phi t)$$

2.3. Fission gas release

The release of fission gas from fuel pellet is important factor in calculation of the gap conductance and internal pressure. The fission gas release expression proposed by Booth shown in Eq. (22) was used in this study:

$$\frac{\partial C_g}{\partial t} = D_g \nabla^2 C_g + \beta_g \quad (22)$$

This equation is subjected to the initial condition: $C_g(r) = 0$ at $t = 0$, and the boundary conditions: $C_g(r = a) = 0$ at $t > 0$, and $\partial C_g / \partial r(r = 0) = 0$ at $t > 0$.

The fraction of gas concentration that reaches the grain boundary with the above boundary conditions is exactly (Millett et al., 2012):

$$f_c = 1 - \frac{6}{\omega} \sum_{n=1}^{\infty} \frac{1 - \exp(-\pi^2 n^2 \omega)}{(n\pi)^4} \quad (23)$$

The diffusion coefficient and gas releasing condition (incubation threshold) described in detail in Shohei et al. (2003) and Bernard et al. (2002), respectively.

3. The IR-FRA code validation

3.1. The Case A

In order to validate the IR-FRA code, the AP1000 reactor fuel rod behavior is considered. The experimental parameters and operating conditions in above case are presented in Table 1. The case is

Table 1
Operating conditions and parameters for the FROBA code (Yu et al., 2012).

Parameter	Value
Average linear power	188 W/cm
Average mass flux	3258 kg s ⁻¹ m ⁻²
Coolant pressure	15.51 MPa
Coolant inlet temperature	279.7 °C
Fill gas initial pressure	2.5 MPa
Heating length	4.27 m
Pitch	1.3 cm
Nominal fuel density	95.5% theoretical
Maximum fuel densification	1% of theoretical density
Gap width	85 μm
Fuel rod diameter	0.95 cm
Cladding width	0.572 mm

simulated by IR-FRA and the results are benchmarked by FROBA code. Fig. 5 depicts the calculated temperatures at the center and surface of fuel and the clad inner wall during burnup. As seen in Fig. 5, the IR-FRA evaluated temperatures profiles appropriately, and its values are close to the FROBA code. However, there is a little difference between them, the major of these differences are related to the dissimilar correlations, models (such as swelling model, cladding creep model) and the oxide layer temperature drop consideration in IR-FRA code. Fig. 6 shows gap width variation during burnup. Initially, fuel expansion lead to gap width decrement. Immediately, it began to increment due to the reduction of fuel density at the beginning of steady operation. When this effect disappeared, the fuel pellet starts swelling gradually. As a result, the gap width starts shrinking until it is eventually closed. Fig. 7 shows the fraction of the released fission gas during fuel burnup. It could be seen that the computed fission gas fraction and incubation threshold are in good agreement with results of FROBA code.

3.2. The Case B

For second test case, in order to validate the IR-FRA code, the study of PWR fuel rods according to report of Fuel and Material Department of Idaho National Lab (INL) is considered. This case was modeled by BISON code (Williamson et al., 2012) which is developed with the INL for analyzing the fuel rod and material. The experimental parameters and operating conditions in above case are presented in Table 2. The case is simulated by IR-FRA and the results are benchmarked by BISON code. Fig. 8 represents the same comparison as Fig. 5 for the second validation case. Figs. 9 and 10 illustrate the gap width and fission gas release that evaluated by the IR-FRA and BISON codes. As shown, the results are bringing together. Although there are some differences between them but the comparison shows the accuracy and applicability of the presented code. It means that the IR-FRA is a reliable numerical code for the predication of the fuel rod behavior during long term burnups.

4. Evaluating the behavior of fuel rod in WWER1000 for the BNPP using the IR-FRA code

In this section, to study fuel rods behavior in the BNPP, a fuel rod of WWER1000 reactor has been assessed by the validated IR-FRA code. The Table 3 shows the design and operating parameters for the fuel rod of WWER1000 reactor. For numerical simulation, the 100 nodes in radial and 10 nodes in axial directions have been

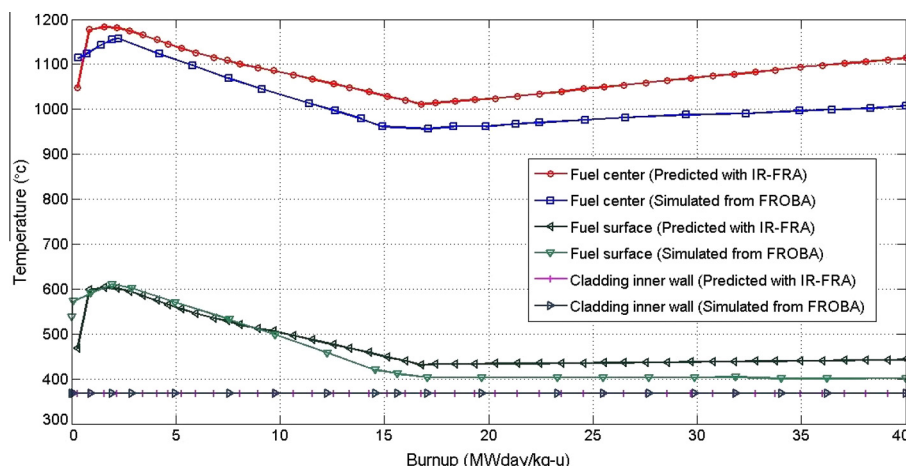


Fig. 5. Comparison of the temperature profiles at the center and surface of the fuel and clad inner wall via burnup (5th axial node from bottom).

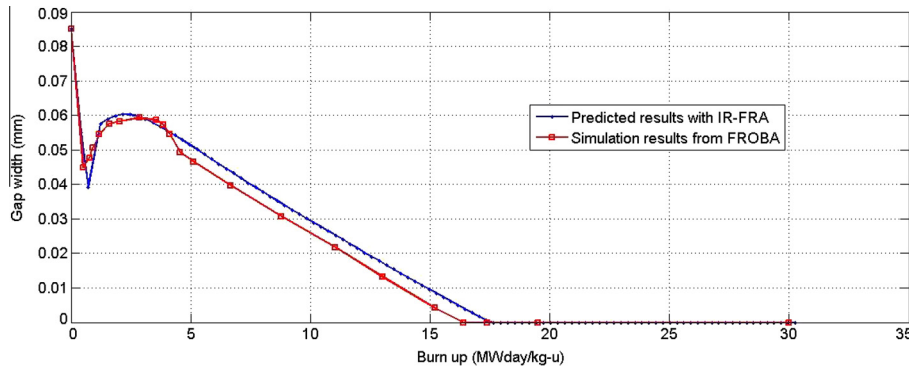


Fig. 6. Comparison of gap width via burnup (5th axial node from bottom).

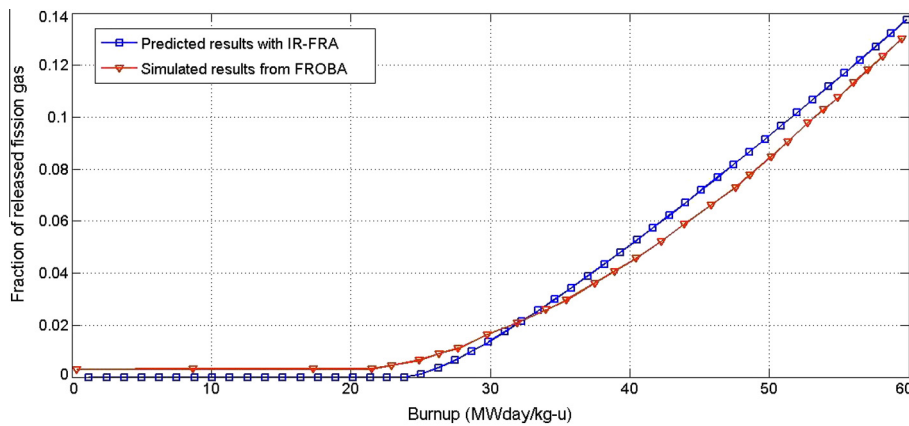


Fig. 7. Comparison of released fission gas via burnup.

Table 2
Operating conditions and parameters for the BISON code (Williamson et al., 2012).

Parameter	Value
Average linear power	200 w/cm
Coolant convection coefficient	7500 W/m ² K
Coolant pressure	15.5 MPa
Coolant temperature (uniform)	530 K
Fill gas initial pressure	2 MPa
Heating length	1.19 m
Nominal fuel density	95% theoretical
Maximum fuel densification	1% of theoretical density
Gap width	80 µm
Fuel rod diameter	0.95 cm
Cladding width	0.57 mm

considered in the model. Fig. 11 shows the temperature contours of the fuel rod for three different burnups (in the onset of steady operation, $Bu = 3.8 \text{ MWd/kgU}$ which the maximum fuel temperature occurs and $Bu = 30 \text{ MWd/kgU}$). In this figure the effect of the fuel burnup on the temperature distributions is board. On the other hand, Fig. 12 depicts the temperature of the bulk coolant, the exterior and interior surface of the clad, and fuel surface along the axial direction. The temperature distribution is in the form of an integral equation, and as the fuel rod height increases, the temperature increases and as the figure shows it goes to 320 °C. The clad surface temperature follows the temperature distribution of the fluid but the temperature of the clad interior surface and the

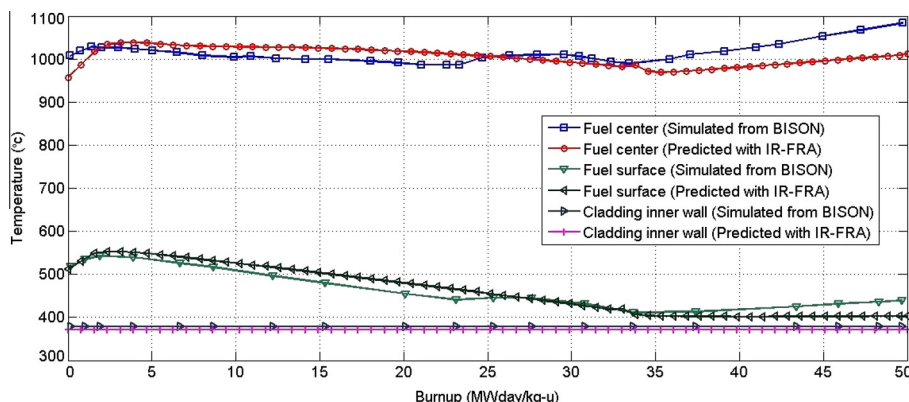


Fig. 8. Comparison of the temperature profiles at the center and surface of the fuel and clad inner wall via burnup (5th axial node from bottom).

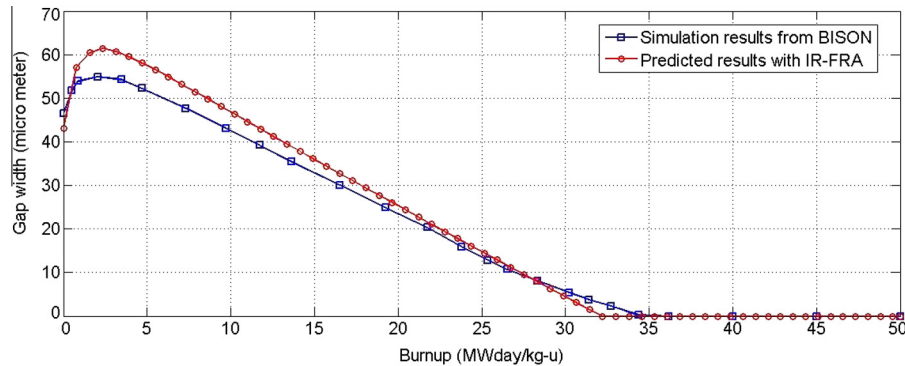


Fig. 9. Comparison of gap width via burnup (5th axial node from bottom).

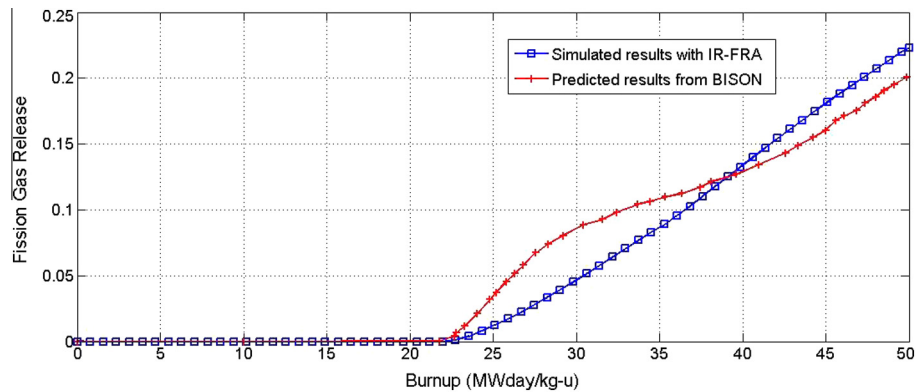


Fig. 10. Comparison of released fission gas via burnup.

Table 3
Main design parameters of WWER1000 fuel rod (FSAR, 2005).

Parameter	Value
Average linear power	170 w/cm
Average mass flux	3850 kg s ⁻¹ m ⁻²
Coolant pressure	15.2 MPa
Coolant inlet temperature	291 °C
Fill gas initial pressure	2 MPa
Heating length	3.58 m
Pitch	1.275 cm
Nominal fuel density	95.5% theoretical
Maximum fuel densification	2.8% of theoretical density
Gap width	80 µm
Fuel rod diameter	0.91 cm
Radius of the fuel pellet	3.785 mm
The volume of the gas plenum	1.8283E-5 m ³
No. of radial segments for fuel	100
No. of radial segments for clad	50
No. of axial segments in fuel rod	10
Burnup at full densification	5 MWd/kgU

fuel surface follow the linear heat rate in the fuel rod height. Figs. 13 and 14 show the variation of gas temperature drop and gap conductance via burnup at different axial locations. With decrement of gap width and increment of gas pressure, the thermal conductance of the filling gas increases. As shown, with gas conductivity increment, the temperature drop decreases. In addition, it is depicted that for the closed gap, regarding contact pressure, the thermal conductance is linearly going up. Fig. 15 illustrates the gap width variation along with the fuel rod height, for some different fuel burnups. It is shown that the gap width varies due

to the different effect of fuel behavior, such as densification, swelling, conductivity, and linear power. Fig. 16 shows the radius of the fuel and clad (interior radius) at fifth axial section (nodes are numbered from bottom). For the sake of comparison, the experimental results proposed by Smirnov et al. (2004) are shown in this figure. The intersection of cladding radius reduction and fuel swelling curves for WWER1000 fuel rods is noticed within the range of about 48–53 MWd/kgU, corresponding the expected moment of contact (Smirnov et al., 2004). As shown, the calculated contact point (50.8 MWd/kgU) is match to this experimental data. Fig. 17 depicts temperature results at the center and surface of the fuel and the clad wall at fifth axial section. As shown, at first the fuel temperature rises quickly due to the fuel densification. When it finished, fuel swelling and cladding creep-down consequences the continuous gap reduction and temperature drop in fuel. At the same time (the gap is close), the fuel centerline temperature began to increase slightly due to the decreasing fuel thermal conductivity. Fig. 18 presents the fraction of released fission gas and the cavity pressure versus the fuel burnup. With increment in gas temperature at the onset of operation, the cavity pressure increases about 2.7 MPa. As expected, the gas pressure is inversely proportional to gap volume (gap volume varies due to the fuel densification and swelling). It could be seen at $Bu = 28.7$ MWd/kgU, when the significant fission gas release begins, the gas pressure rising goes dominant. The fuel rod length experiments different operating condition. Therefore, the oxide layer thicknesses at different axial locations are dissimilar. The oxide layer thickness variation via burnup is shown in Fig. 19. Cladding oxidation occurs in three stages. The rate of oxidation which is scribed by Eqs. (3)–(5) varies in each state. This matter is board in Fig. 19. Fig. 20 depicts the var-

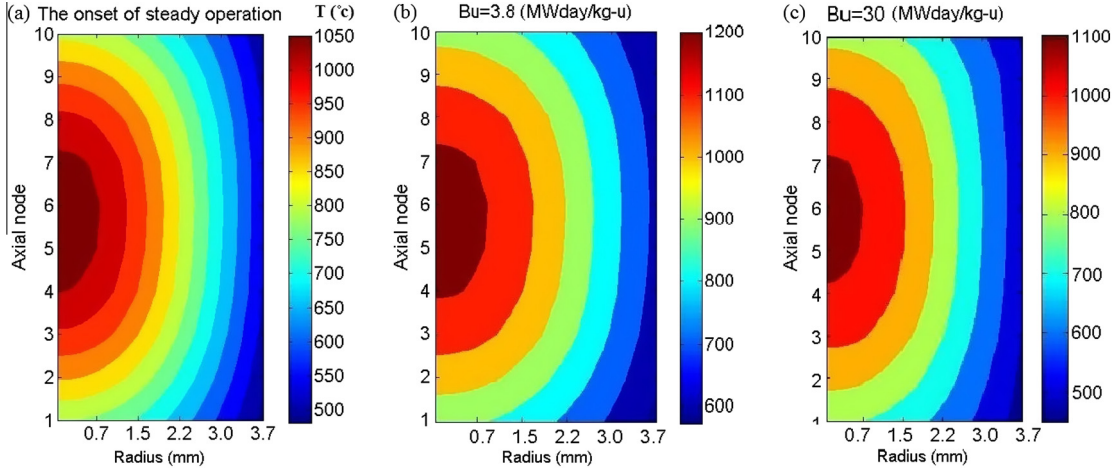


Fig. 11. The fuel temperature contours via burnup for WWR1000 fuel rod in BNPP.

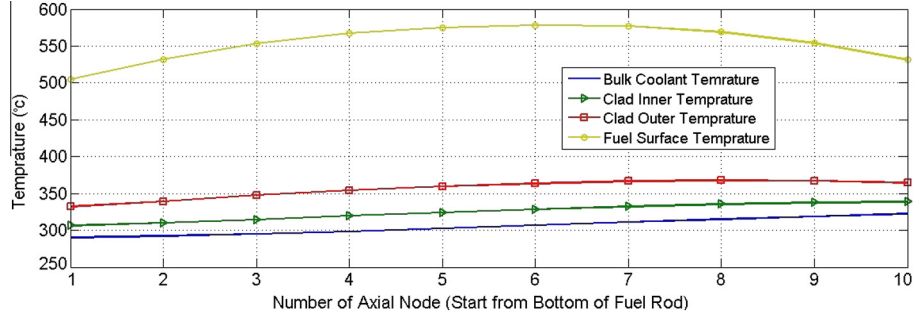


Fig. 12. The coolant, fuel (outer) and cladding surface (inner and outer) temperatures in axial direction for WWR1000 in BNPP.

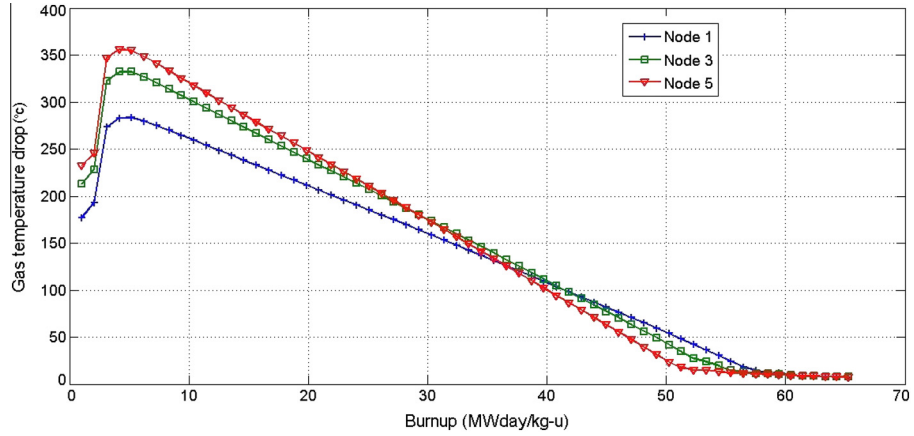


Fig. 13. The gas temperature drop via burnup for WWR1000 fuel rod in BNPP (axial nodes 1, 3, 5 from bottom).

iation of pellet surface hoop strain at different axial locations. At initial stages, the hoop strain is negative because of fuel densification. It increases after the densification due to the fuel swelling. Fig. 21 shows the axial stress of the pellet surface at different axial locations. At the first, with thermal expansion of fuel, the axial stress sign is positive. It began to decrease due to the fuel densification. Once the densification is getting complete, axial stress increases slowly due to fuel swelling. Figs. 22–24 show the displacement, radial stress, and hoop stress of the fuel in some

axial locations, respectively. These figures are depicted for very low burnups. The fuel pellet displacement computed with principle of virtual work is shown in Fig. 22. This displacement are appeared from the thermal expansion and the pressures that applied to the fuel. Fig. 24 shows the hoop stress on the fuel. As shown, because of the gradient of the temperature, the central part of fuel is under pressure and outer is under tension. Therefore, the outer part of the fuel cracks at the beginning of the reactor work.

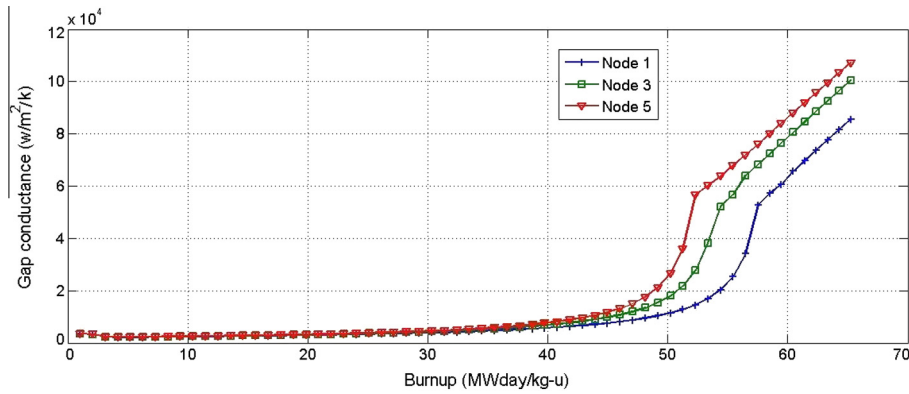


Fig. 14. The gap conductance via burnup for WWER1000 fuel rod in BNPP (axial nodes 1, 3, 5 from bottom).

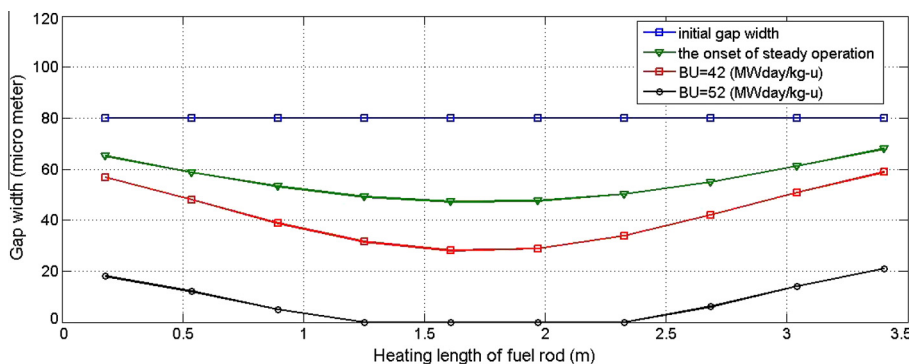


Fig. 15. The gap width via burnup for WWER1000 fuel rod in BNPP.

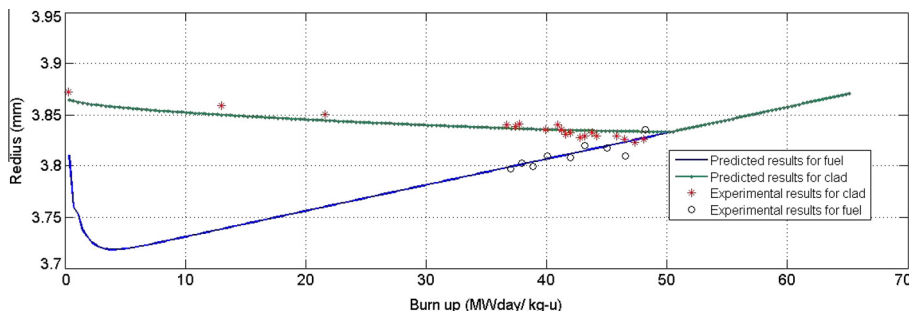


Fig. 16. The fuel (outer) and clad (inner) radius via burnup for WWER1000 fuel rod in BNPP (5th axial node from bottom).

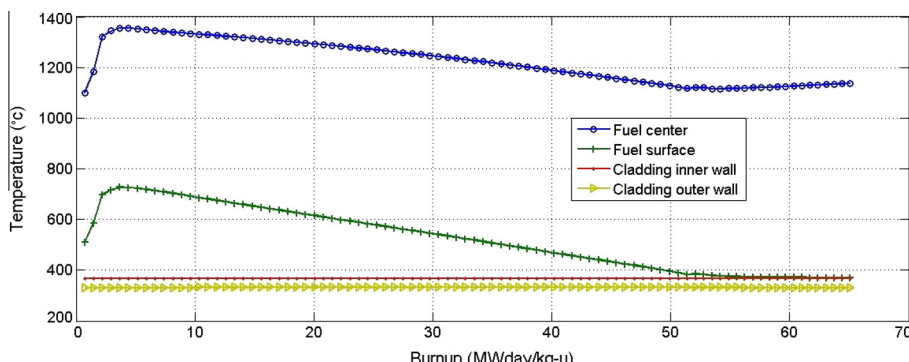


Fig. 17. The fuel (center and surface) and clad (inner and outer) temperatures via burnup for WWER1000 fuel rod in BNPP (5th axial node from bottom).

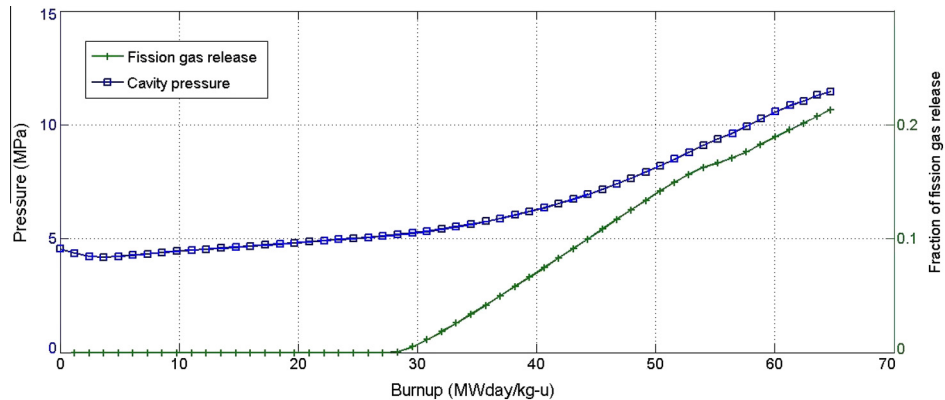


Fig. 18. The predicted total released fission gas and the cavity pressure via burnup for WWER1000 fuel rod in BNPP.

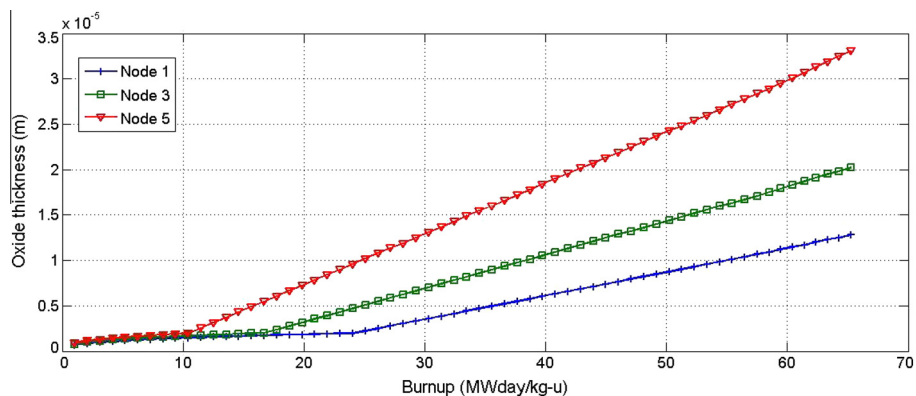


Fig. 19. The oxide layer thickness via burnup for WWER1000 fuel rod in BNPP (axial nodes 1, 3, 5 from bottom).

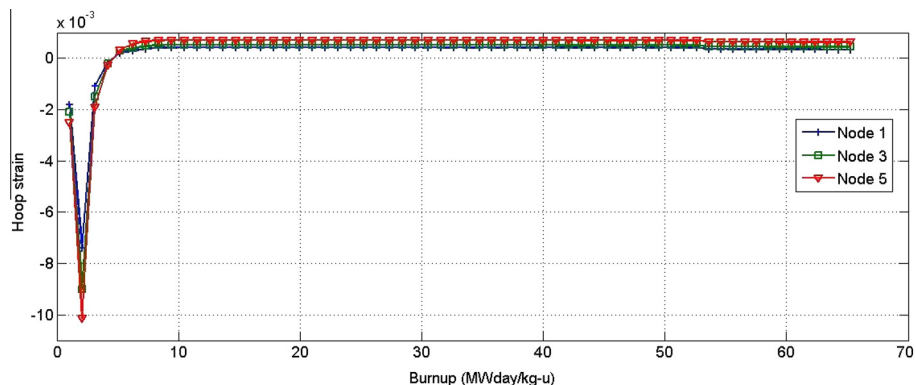


Fig. 20. Pellet surface hoop strain via burnup for WWER1000 fuel rod in BNPP (axial nodes 1, 3, 5 from bottom).

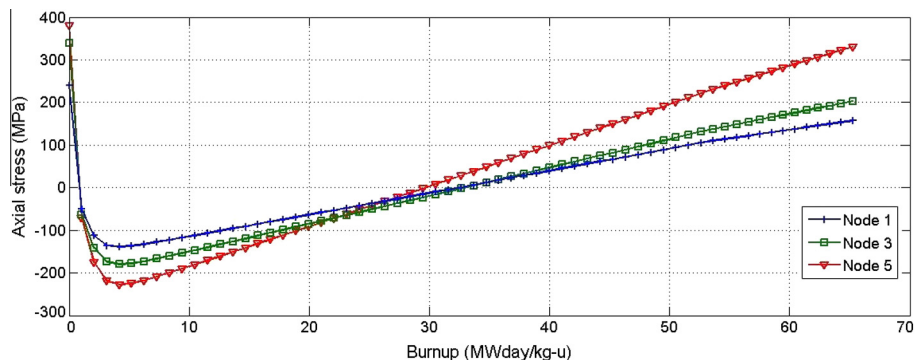


Fig. 21. Pellet surface axial stress via burnup for WWER1000 fuel rod in BNPP (axial nodes 1, 3, 5 from bottom).

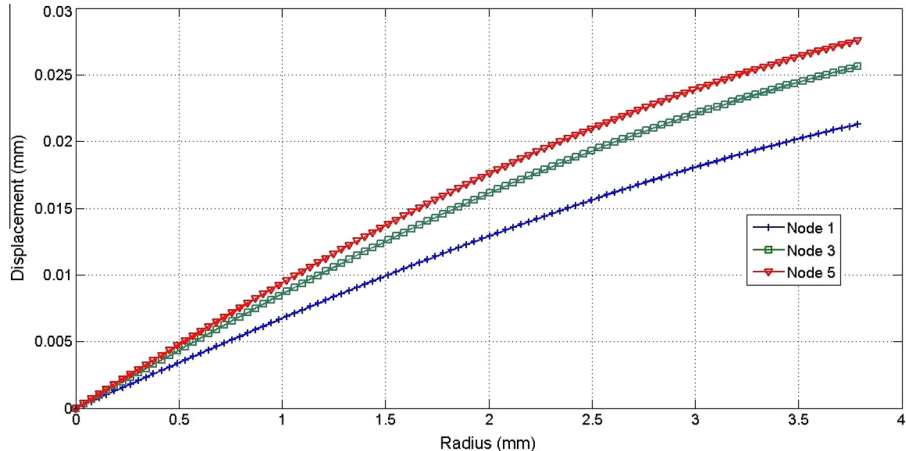


Fig. 22. Radial displacement in the center of fuel pellet via burnup for WWER1000 fuel rod in BNPP (axial nodes 1, 3, 5 from bottom).

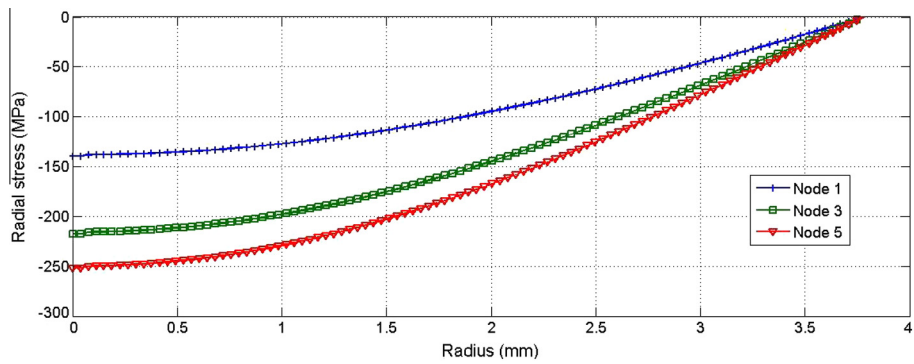


Fig. 23. Radial stress in the center of fuel pellet via burnup for WWER1000 fuel rod in BNPP (axial nodes 1, 3, 5 from bottom).

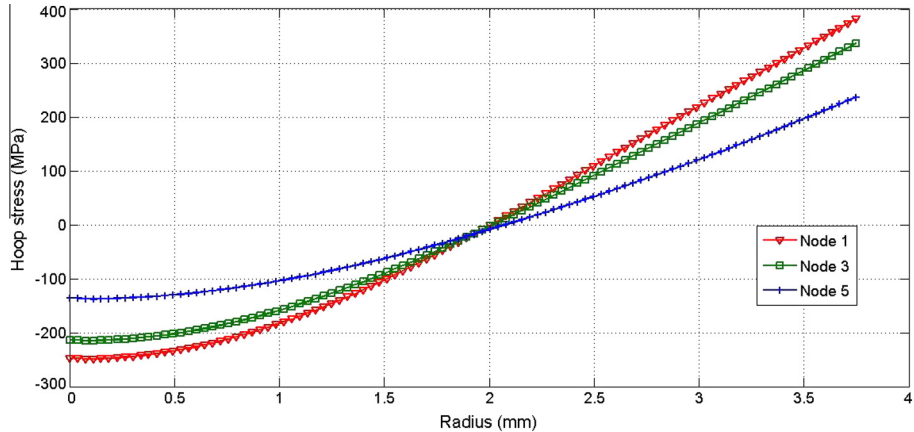


Fig. 24. Hoop stress in the center of fuel pellet via burnup for WWER1000 fuel rod in BNPP (axial nodes 1, 3, 5 from bottom).

5. Conclusion

In this work, the IR-FRA code was developed for studying fuel rod behavior under long-term burnups. It is shown that it could be used for predicting the pellet-clad mechanical interaction. In addition, the other operating parameters like fuel, clad and coolant temperatures, gas pressure, stress and displacement in all domain could be drawn out from this code. The ability to choose different numerical solution methods for mechanical and thermal analysis (finite difference, finite element, analytical methods) is another advantage of this code. Also, the virtual work theory base on finite

element method is introduced as an efficient method for fuel displacement calculation. At first, the accuracy and reliability of the code was demonstrated in several stages. The code was validated against the FROBA and BISON codes and experimental data. The acceptable agreement with presented data demonstrated this validity. Afterward, the WWER1000 fuel rod behavior in the BNPP was evaluated with the IR-FRA code and important parameters such as the stresses, contact point, displacement, gap conductance, gap width and fuel centerline temperature were presented. Generally, from this simulation the following conclusions are obtained:

- It is revealed that the fuel-clad mechanical interaction occurs after 1200 days (about 50 MWd/kgU) and the results are consistent with experimental data (WWER1000).
- According to the comparisons between gap width and point of contact (WWER1000 and AP1000 cases) the importance of densification in delaying the contact point could be realized.
- Comparison of the fuel-clad contact with experimental data (WWER1000 case) confirms cladding creep, densification and swelling models in this code.

Acknowledgement

The authors are grateful for the support of Shahid Beheshti University.

References

- Allison, C.M., Berna, G.A., Chambers, R., 1993. SCDAP/RELAP5/MOD3.1 Code Manual Volume IV: MATPRO—a Library of Materials Properties for Light-Water-Reactor Accident, Analysis. NUREG/CR-6150.
- Berna, G.A., Beyer, C.E., Davis, K.L., 1997. FRAPCON-3: A Computer Code for the Calculation of Steady-State, Thermal-Mechanical Behavior of Oxide Fuel Rods for High Burnup. NUREG/CR-6534-Vol. 2. System Technology Office of Nuclear Regulatory Research, Washington.
- Bernard, L.C., Jacoud, J.L., Vesco, P., 2002. An efficient model for the analysis of fission gas release. *J. Nucl. Mater.* 302, 125–134.
- Russia Federal Agency on Nuclear Energy (RFANE), 2005. Final Safety Assessment Report (FSAR) for BNPP. Book 1, Moscow.
- Garcia, P., Struzik, C., Agard, M., Louche, V., 2002. Mono-dimensional mechanical modelling of fuel rods under normal and off-normal operating conditions. *Nucl. Eng. Des.* 216, 183–201.
- Herranz, L.E., Feria, F., 2010. Extension of the FRAPCON-3.3 creep model to dry storage conditions. *Prog. Nucl. Energy* 52 (7), 634–639.
- Hikmet, S.A., Pedro, O., 2005. A review of nuclear fuel performance codes. *Prog. Nucl. Energy* 46, 127–141.
- Hongxing, Y. et al., 2012. Development of Fuel ROd Behavior Analysis code (FROBA) and its application to AP1000. *Ann. Nucl. Energy* 50, 8–17.
- Kramman, M.A., Freeburn, H.R., 1987. ESCORE—the EPRI Steady-State Core Reload Evaluator Code: General Description, EPRI NP-5100. EPRI, Palo Alto, CA.
- Lucuta, P.G., Matzke, H., Hastings, I.J., 1996. A pragmatic approach to modelling thermal conductivity of irradiated UO₂ fuel: review and recommendations. *J. Nucl. Mater.* 232, 166–180.
- Millett, P.C., Tonks, M.R., Biner, S.B., 2012. Grain boundary percolation modeling of fission gas release in oxide fuels. *J. Nucl. Mater.* 424 (1–3), 176–182.
- Rashid, Y., Dunham, R., Montgomery, R., 2004. Fuel analysis and licensing code: FALCON MODO1, EPRI Report 1011308.
- Ross, A.M., Stoute, R.L., 1962. Heat transfer coefficient between UO₂ and Zircaloy-2, Atomic Energy of Canada Technical Report, AECL-1552.
- Shohei, U., Junya, S., Koichi, E., 2003. Fuel and fission gas behavior during rise-to-power test of the high temperature engineering test reactor (HTTR). *J. Nucl. Sci. Technol.* 40, 679–686.
- Smirnov, A.V., Markov, D.V., Ovchinnikov, V.A., Polenok, V.S., Ivashchenko, A.A., 2004. Pellet-cladding interaction in VVER fuel rods. In: Pellet–Clad Interaction in Water Reactor Fuels, France.
- Todreas, N.E., Kazimi, M.S., 1999. Nuclear System I, Thermal Hydraulic Fundamentals. Taylor & Francis, pp. 332–338.
- Williamson, R.L., 2010. Simulation of NGNP Fuel using the BISON Fuel Performance Code. Progress Report. Technical Report INL/EXT-11-21403, Idaho National Laboratory.
- Williamson, R.L., 2011. Enhancing the ABAQUS thermomechanics code to simulate multipellet steady and transient LWR fuel rod behavior. *J. Nucl. Mater.* 415 (1), 74–83.
- Williamson, R.L., Hales, J.D., et al., 2012. Multidimensional multiphysics simulation of nuclear fuel behavior. *J. Nucl. Mater.* 423 (1–3), 149–163.
- Yu, H. et al., 2012. Development of Fuel Rod Behavior Analysis code (FROBA) and its application to AP1000. *Ann. Nucl. Energy* 50, 8–17.